Seasonal monitoring of environmental tracing combined with one-time multi-tracer test survey: an efficient method to establish groundwater conceptual model of large landslide in spatial sparse data context (Séchilienne, French Alps)

Vallet A., Bertrand C., Mudry J., Bogaard T., Vengeon J.M., Baudement C., Régent B.

1. Introduction

If gravity is known as the main factor in landslide motion, water has a prominent triggering role in its dynamics. Increase of groundwater level play an important role in the (re)activation of deep-seated slope movements (Van Asch et al., 1999; Iverson, 2000; Rutqvist and Stephansson, 2003) and many studies attempted to characterize water infiltration-destabilisation relationship (Alfonsi, 1997; Belle et al., 2013; Chanut et al., 2013; Corominas et al., 2005; Helmstetter and Garambois, 2010; Hong et al., 2005) or to model hydro-mechanical coupling (Bonzanigo et al., 2001; Cappa et al., 2004, 2006; Guglielmi et al., 2005; Ronchetti et al., 2010; Sun et al., 2009). However, such approaches, to be accurate and to reflect field conditions, require to be based on a relevant groundwater conceptual model.

Most of deep-seated landslides have a well-developed destabilisation monitoring network with numerous stations and various technologies involved (extensometer, radar, LIDAR, infrared, pictures…). Along, landslide geology is generally well known, thanks to structural mapping and geophysical investigation. On the contrary, groundwater investigation is made difficult by the sparse density of natural or artificial points of hydrogeological interest. First able, direct and local measurements of water pressure (such as piezometers) are hardly representative, because of the dual-permeability rock mass heterogeneity and discontinuity and the large rock mass volume involved in the destabilization (millions of cubic meters). Secondly, due to landslide displacements borehole has a short life span (damage).

For all these reasons, classical hydrogeological methods, such as piezometry, are not appropriate and hydrogeological investigation focused recently on natural and/or artificial tracer monitoring (Binet et al., 2007; Bogaard et al., 2007; Guglielmi et al., 2002; Vengeon, 1998). This is a transversal method which has proved its worth for heterogeneous aquifer investigation such as karst (Bakalowicz, 1979; Mudry, 1987). However, indirect information of landslide groundwater provided by spring monitoring is also often difficult to implement. Indeed, most of deep-seated unstable near surface zone is highly deconstructed, favouring infiltration and enabling to settle perched aquifer, of which groundwater often flows toward a valley floor alluvial aquifer through the landslide foot scree cone. As a result, generally very few springs (even none) are located on the unstable area and hydrogeological investigation has to focus on springs surrounding the landslide with no possibility of water-balance computation.

Because hydrochemistry surveys are time-consuming and expensive, and as landslides are mainly monitored by non-hydrogeologists, many landslide studies are based on few temporary scattered field campaigns, in order to have a snapshot of the hydrogeological conditions. On the contrary, a dedicated hydrogeological study, often performed on site, providing more comfort access to groundwater information, monitors a wide range of parameters, including water-level, on the long term, enabling extensive analysis (Cervi et al., 2012). This study aims at showing that an intermediate level of investigation can allow to determine accurately and efficiently or to refine a groundwater conceptual model. The proposed method combines three complementary approaches, (i) one-time multi-tracer test survey during high water level period, (ii) seasonal monitoring of water stable isotopes and electrical conductivity, and (iii) a hydrochemical survey during low water periods, respectively, to determine, (i) flow path and residence time, (ii) average recharge elevation and hydrodynamic behaviour, and (iii) water clusters and then water origin.

2. Material and methods

2.1. Method

2.1.1. Motivation: sparse data context

Deep seated landslides mainly occurs in crystalline bedrock where takes place fractured rock aquifers (Binet, 2006). This type of aquifer has the particularity to have permeability properties. Depending on fractures' degree of aperture, connectivity and density, they can be highly transmissive (transfer function) or more inertial and then play the role of storage reservoir (essentially matrix cracks/interstices network, named micro-fissured blocks for the rest of the article). Fractured rock aquifers are heterogeneous and anisotropic media with rapid water flow in discontinuities bypassing the less pervious micro-fissured blocks (Bogaard et al., 2007). As a consequence, hydrogeological measurement (such as permeability or water-level) is highly dependent on the observation scale (ranging from millimetres to kilometres, depending on the discontinuity type: local fracturing, foliation, or major tectonic discontinuities; (Clauser, 1992), a local measurement being not representative of the aquifer behaviour. Additionally, in mountainous context, a vertical hydraulic conductivity gradient occurs as sub-surface medium is more decompressed, with values ranging from 10^{-11} to 10^{-5} m/s toward the surface (Maréchal and Etcheverry, 2003). This characteristic is enhanced in the unstructured landslide zone. Bedrock sedimentary cover layers (such as carbonate, colluviums) can also lead to hydraulic conductivity disparity. Both mentioned permeability contrasts can be sufficient to support perched aquifer (Binet, 2006; Tullen, 2002).

2.1.2. Tool: Artificial and natural tracers

Anisotropy and heterogeneous medium combined with landslide deformation make traditional hydrogeology investigation, mainly based on local borehole, difficult even unsuitable, leaving the open-ended question of measurement representativeness. Artificial and natural tracer methods have the advantage of being non-intrusive and to provide global informations at the aquifer scale (Guglielmi et al., 2002). Hydrochemistry signals are influenced by groundwater flow path through different lithology types and by aquifer hydrodynamic behaviour. In low water period, groundwater flow is essentially driven by aquifer drainage with low external disturbance (low recharge), unlike the high water period. As a consequence, hydrochemistry of water spring reflects the water-rock interaction and provides information about water origin, residence time and flow path. From another side, analyze of signal seasonal variations (seasonal pattern, dispersion, magnitude….) enable to characterize the aquifer hydrodynamic behaviour. These fluctuations inform how much the spring is recharged by rock crack/interstice (inertia) and/or transmissive fracture network (reactivity). Last, but not least, groundwater chemistry is also closely related to landslide hydromechanical processes, therefore landslide deformation can modify the hydrochemical response (Binet et al., 2009) and makes it possible to distinguish water which has flowed through the unstable area or not. Conservative natural tracers such as water stable isotopes allow to determine water average elevation and to follow seasonal changes revealing different degree of fracture network connectivity. Artificial tracers enable to determine flow paths, directions and velocities. Artificial tracers are complementary of natural tracer survey, as they allow to test hydrogeological connection hypothesis by investigation of the contribution of spatially constrain area (injection point). Among artificial tracer, fluorescent tracers are the most popular thanks to high sensitivity analysis, low detection limit (small tracer amount needed), and toxicity level low to null (Leibundgut et al., 2011).

2.1.3. Implementation: seasonal approach

One-time multi-tracer test survey was performed in springtime during snowmelt period, which is the highest recharge period. It is crucial to characterize this period as it is the worst period for destabilization of rainfall triggered landslides and also as high groundwater level can enable the water to flow through a new pathway (fracture connectivity), modifying groundwater flow path which will not occur in low water season. Finally, working in recharge period allowed maximizing the probability to retrieve tracer concentration at a detection level at resurgence points. The main purpose of the tracer-test survey is to test hydraulic connection hypothesis and to raise the doubt from the conceptual model draft. Along for each spring, a unique average recharge area elevation was estimated by averaging all results of stable isotopes seasonal survey. This method is complementary to tracer test, as stable isotope gives the origin of water on average, with no information about transit time, whereas tracer test informs about only one of the possible flow path to the springs but with velocity quantification for the fastest flow component. Hydrochemistry survey was only performed in low water period, enabling to separate different clusters of water, due to their different geochemical conditions (water-rock interaction, residence time…) and to confront them with massif lithology to reconstruct their origin, independently from recharge influence.

Finally, a seasonal analysis was performed by comparative review of natural tracer signal variations, in order to deduce springs relative hydrodynamic behaviour (and not absolute). This analysis allows to differentiate springs more or less insensitive to seasonal conditions (inertial aquifer) and others very reactive (reactive aquifer), and also to identify seasonal pattern (dilution, drainage mechanism). This seasonal analysis is based on a conservative (stable isotope) and non-conservative tracer (electrical conductivity), to characterize drainage network extension and sensitivity to recharge, respectively. Electrical conductivity was used, instead of cation and anion concentrations, as for this analysis a measurement representative of water total mineralization is sufficient and cost effective. The combination of these four approaches (tracer test, stable isotope, hydrochemistry and seasonal analysis) bringing all complementary informations, and allows to well constrain the groundwater conceptual model.

Hydrochemistry data and conceptual model from Vengeon (1998) and Guglielmi et al. (2002) were used as baseline to select the injection locations, the springs to monitor and the sample rate. For other sites, devoid of preliminary studies, it is strongly recommended to perform at least two hydrochemistry snapshots, respectively in high and low water periods, in order to produce a first draft of the site conceptual model, which will serve as the basis to the design of the investigation protocol. Multi-tracer test was performed in two stages, in April 2001 and 2002. Four isotopic campaigns were performed quarterly (November-December 2011, January-March 2012, April-June 2012 and July-September 2012). 5 hydrochemistry surveys were performed in low water period. Electrical conductivity was measured for 5 more surveys in high water period.

Except tracer tests, all the surveys spread from September 2010 to September 2012. It is worth mentioning that the Séchilienne site have the particularity to include five galleries (four of them are located in the unstable area), which were investigated for this study (fracturing and water inflow survey). Information gathered in the galleries and their 3D spatialization enables to locate the approximate depth of the water level within the unstable slope.

2.2. Site

To take stock of the relevance of the chosen method, this study focused on the Séchilienne deep-seated unstable slope. The Séchilienne landslide is located on the right bank of East-West flowing Romanche River, near the South eastern side of the city of Grenoble (Isère, France). The landslide is located on the southern slope of the Mont-Sec and l'Oeilly Peak Mountain which has a maximum elevation of 1547m. This mountain corresponds to the SW border of the Belledonne alpine massif. This landslide is particularly advantageous, as it has already been investigated by two distinct snapshot hydrochemistry surveys, but only the unstable slope has been investigated and the interactions with the surrounding environment were disregarded. In addition, groundwater flow mechanisms that are responsible for recharge of the disturbed zone are still in debate in the scientific community. Vengeon (1998) shows that the disturbed zone perched aquifer is recharged by water-level rise of the deep saturated zone whereas Guglielmi et al. (2002) shows that the main recharge originates from the top sedimentary perched aquifer. Conclusions are mainly based on basic modelling assumption, rough water-balance estimation, geology observation and low field hydrogeology data density to constrain the design of the conceptual model. The second reason why the Séchilienne site was chosen is its spatially sparse hydrogeological network. Indeed, no springs are present in the unstable zone. Only three galleries, located in the disturbed zone, enable water leakage or water inflows monitoring. In addition, the surrounding springs of the massif are subjected to high anthropic pressure (private or public water diversion) which makes impossible yield measurements as only overflow is available, preventing water balance. The above method aims at raising the doubt about uncertainties of the groundwater flow paths and rainfall-triggered mechanism, which will allow extensive studies on the Séchilienne site as hydromechanical modelling.

2.2.1. Massif and landslide geology

The massif can be divided into a metamorphic basement, mainly composed of micaschists alternating with fine-grained gneisses and chloritic schists, oriented N-S/90°, and an unconformably lying sedimentary cover including Lias to Carboniferous deposits (Pic de l'Oeilly). This unconformity also defines the top east landslide summit scarp at about 1100m. Finally, scree and fluvio-glacial deposits locally cover the basement and sedimentary deposits in the upper part of the Mont Sec massif (Guglielmi et al., 2002). Micaschists mainly consist of quartz, biotite, white mica (phengite) and chlorite with occurrences of granoblastic quartz-feldspar (albite in composition) mass, carbonate veins, and disseminated pyrite. After all, pyritic black shales alternating with more or less leucocratic gneiss can be observed. Liassic deposits essentially consists of limestones with intercalation of breccias-rich bands containing pebbles of coal, micaschists and dolomites, while Triassic is represented from its base to the top by sandstone, quartzite, dolomite and intercalation of black shales and argilites. Carboniferous deposits are characterized by micaceous black shales, sandstones and conglomerates with intercalation of anthracite (Barféty et al., 1972; Vengeon, 1998). The unstable slope is delineated to the East by a N20° trending major fault zone. The slope is cut by a dense network of sub-vertical continuous fracture sets, striking N50-70° (Vengeon, 1998). The latter divides the slope into numerous sub-vertical stripe/block compartments. To a lesser extent, the slope has a large number of sub-vertical discontinuous fractures, sub-parallel and dipping slightly toward the valley (Vengeon, 1998).

2.2.2. Unstable slope mechanism and rainfall triggering

The particular importance of the Séchilienne unstable slope is the absence of a significant basal sliding surface. The Séchilienne unstable slope has deep seated progressive deformation controlled by the main discontinuities. The slope is affected by a toppling movement of the N50-70° striking blocks toward the valley coupled with the subsidence of the upper part of the slope near Mont Sec (flexural toppling). The landslide velocities smooth over progressively toward the west and the slope foot, whereas the velocity drops abruptly beyond the N20° trending fault zone delimiting the East boundary. The Guglielmi et al. (2002) hydrogeochemical survey showed that the top sedimentary deposit holds a perched aquifer. As well, the disturbed zone, about 150 m deep (Le Roux et al., 2011), shows a high hydraulic conductivity in comparison with the bedrock (Vengeon, 1998) and constitute a perched aquifer. Indeed, the deformation has caused wide opening of the fractures. Séchilienne unstable slope shows a good correlation between antecedent cumulative gross rainfall and average displacements (Rochet et al., 1994; Alfonsi, 1997; Chanut et al., 2013). Helmstetter and Garambois (2010) showed a weak but significant correlation between rainfall signals and rock fall micro-seismicity. Recently, Vallet et al (2013) showed that Séchilienne displacement rate is better correlated to effective rainfall than gross rainfall, reinforcing the significant role of groundwater flow in the Séchilienne destabilization. Instability in the Séchilienne slope is mainly triggered by rainfall events however other triggers, such as seismic events, are not insignificant (Grasso et al., 2013).

2.2.3. Monitoring network

Among the 30 springs identified across the Séchilienne massif (Fig. 1), none is located on the unstable area as they all surround it. However, a mine gallery and a survey gallery, both located on the unstable zone, show water inflow and/or leakage workable for monitoring, respectively G585 and G710. Unfortunately, the G585 is not any more accessible and was only sampled by Vengeon and monitored for tracer test surveys. In addition, gallery EDF outlet (GEDF), Romanche River (RO1 and RO2) and Rif Bruyant Stream (RIB) have been punctually added to the monitoring network. As well, gallery EDF had been also monitored for water chemistry (CETE, 1993) and for tracer-test survey (2002). GEDF has been survey only occasionally because maintenance emptying happens only once a year. Séchilienne has a strong anthropic pressure, with many public and wild private water supply springs, which makes improbable spring flow estimation. Most of the monitored spring flows were the overflow leftover from water withdraws (DHU, RNE, COR, MOU, MTJ, BAT, THL, MAT, FON, FIN, CBE), not representative of aquifer drainage, being a single point in multiple resurgence area, (VIZ1, VIZ2, VIZ3, VIZ4, CMJ, AIL, THE, PLE, G585-1) or water leakage collected with cover (G710-1, G710-2, G585-2, G585-3). Gallery G900, which is dry, was used only for tracer test survey. Demolition works of a hydro power plant, after tracing survey, have modified flow path of NCH which is probably currently flowing directly to alluvial aquifer. CLO and MUL were only monitored for the tracer test survey. Finally, five rain collectors were installed at about 200 m elevation difference (G710, FON, MAD, ROC and PIO), of which two were coupled with a lysimeter (G710, MAD), covering the massif spatial extension and elevation range.

2.3. Tracer test survey

A 4-tracer test survey was implemented in April 2001 on the Séchilienne unstable slope watershed. Four different fluorescent tracers were injected at four different strategic locations.

Injection locations were selected upon the conditions that (i) location should have preferential infiltration properties and (ii) that spatial location was a special interest point to improve understanding of groundwater flow scheme. Tracer tests survey settings should improve understanding of (i) extension of the recharge area of the unstable slope, (ii) role of the top sedimentary cover in the groundwater flow, (iii) role of the recharge on the unstable slope area and (iiii) hydraulic conductivity between landslide sub vertical stripes. The location selection was based on geomorphology, hydrogeology and geology criteria.

The Rochassier sinkhole (ROC), located on the Sabots fault, was selected to represent infiltration on the top sedimentary cover. In addition, the Rochassier sinkhole was also selected as it was sufficiently remote from the landslide to evaluate extension of the recharge area. 8 kg uranin, pushed by 3 m^3 of water pumped in a neighbouring pond have been injected. A crevasse located in a counter slope sector, at the foot of the Mont Sec escarpment, subsidence part at the top of the landslide, was chosen to represent infiltration on summital landslide area (CRE). 5 Kg rhodamin B, pushed in the underground by 8 m^3 of water pumped in the Mont-Sec pond have been injected at the foot of the highest settlement of the ground in the unstable area. The tracer was injected in a close depression in the mica-schist. Another close depression, situated in the middle part of the unstable area, just few meters lower than the mine gallery 900 has been chosen to test sub vertical stripes conductivity (G900). 6 kg of Sodium Naphtionate have been driven forward by a low flow derived from the Rivoirands water supply pipe (estimated 30 m^3). A sink in the mine gallery 585 (G585-1), which is located eastwards of the rock fall corridor on the eastern side of the landslide, marked by N20 striking major faults has been chosen to characterize landslide recharge and behaviour of this eastern most active part of the slope. At the bottom of this mine gallery, a perennial low flow (about 0.05 L/s) seeps into an open crack. 5 kg of Eosin have been injected in this fracture, pushed by the natural water flow.

As the precise breakthrough points couldn't be determined, being inside the EdF gallery, another tracer test has been performed with uranin injected in the crack, as soon as the gallery has been emptied for maintenance (March, 2002), in order to locate the breakthrough points along the EdF gallery. For both tracer tests, due to the impossibility to estimate monitoring point water flow, only shortest way and breakthrough time were deduced from tracer test survey (no breakthrough curves).

24 points were monitored for the multi-tracing survey of 2001. G585, DHU and RNE springs were monitored with an automatic sampler. Activated charcoal packets and manual water sampling were implemented at FON, CBE, FIN, MAT, THB, MTJ, COR and from VIZ1 to VIZ4 springs. Only charcoal monitoring was performed on the remaining springs. Monitoring survey stood for two months, and sample rate was adapted according to survey time by decreasing sampling resolution. In the reiterated tracer test from gallery 585 (2002), only hand samplings have been performed in each water inflow of the EdF gallery, between kilometric points 5 and 7 (Fig. 2E).

2.4. Oxygen stable isotopes

Water stable isotopes fractionation is thermo-dependent and is higher at low than at high temperature for water/vapour equilibrium exchange (Clark and Fritz, 1997). This properties combined with other hydrological process yield to a series of macroscale effects on the isotopes fractionation (continental effect, latitude effect, seasonal effect and elevation effect) (Leibundgut et al., 2011). Isotopic abundance ratio of a water sample (this study used δO^{18}) is determined according to an international acknowledged standard (the so-called V-SMOW) and is expressed in ‰. At this study scale (local), only elevation and seasonal effects have a non-negligible impact on oxygen isotope gradient. Elevation effect is the result of fractionation thermo-dependency and water vapour condensation by adiabatic cooling and as for consequences a δO^{18} depletion of precipitation at higher elevation. Seasonal effect can be the consequences of numerous factors, such as air masses circulation or atmospheric conditions, but it is globally linked to the air temperature seasonal variation. Depending on site, seasonal effect can significantly impact and modify the elevation effect through the year which becomes seasonally dependent. Finally, infiltration isotopic signal can be then modified from precipitation through the soil layer by evaporation process which lead to δO^{18} enrichment (Gat, 1996).

2.4.1. Isotopic gradient

Determination of the local elevation effect (Elevation = a * δO^{18} + b) makes oxygen stable isotopes a powerful tool to design hydrogeological conceptual model. Indeed, a representative sampling of site water inflows (spring, gallery seepage…) enables determination of their average recharge altitudes. Such an assignation, to be accurate, requires nevertheless a precise knowledge of the local isotope gradient. In mountainous contexts, a local calibration is generally possible, using springs located on the slope, whose recharge area is well defined and limited with height difference. At Séchilienne, no well-known springs allow this approach. Instead, a set of rain collectors and lysimeters have been installed. To determine the isotopic elevation gradient on Séchilienne watershed site, five rainfall collectors, of which two were coupled with a lysimeter, were implemented to characterize O^{18}/O^{16} isotopic signal related to elevation, respectively for precipitation (rainfall and snowmelt) and infiltration hydrosystem inputs. Collection points were installed with an average elevation difference of 200 meters from 640 to 1520 m asl, and with a large spatial distribution, both covering most of the massif bearing the landslide (Fig. 1). Hermetic rain collector tanks were buried about one meter deep and wrapped with an isotherm cover to avoid isotope fractionation due to atmosphere temperature fluctuation. The Madeleine and G710 lysimeters were installed respectively in grassland and woodland, the two main vegetation types of the watershed. Precipitation isotopic gradient was firstly determined with the 5 rain collectors. In order to determine the infiltration isotopic gradient, precipitation isotopic gradient was shifted to fit the lysimeter spots, assuming that evaporation is homogeneous on site and shifts positively only the intercept of the gradient whereas slope is kept identical.

2.4.2. Spatialization

As explained in chapter 2.3.1, Séchilienne massif has a strong anthropic pressure and it was not possible to estimate spring flow. As a consequence, it was not possible to assess recharge area extension using the spring flow and precipitation amount and performed extensive analysis. Instead, a simple method to spatialize data was implemented. For each outlet, the steepest slope line was determined until the ridge line based on a digital elevation model of 25 meters resolution. To simplify the visualization, the line joining the spring to the intersection of the ridge line and steepest line was drawn for each spring. Elevations along this line constitute an approximation of the elevation range if spring would have a local recharge area explained by topography. If elevation range of the steepest slope line was able to explain δO^{18}elevation value, then the recharge area was considered as local. Otherwise, ridge line was used to match up the δO^{18} elevation and approximate spatial position of recharge area.

2.4.3. Sampling proceeding

Water which comes out of springs does not match with the last rainfall period. Residence time, hydrosystem inertia and hydraulic connectivity, mix, delay and buffer rainfall signal. Moreover, isotopic elevation gradient varied in time as it depends of rainfall temperature condensation (depending on season). Therefore, an O^{18}/O^{16} synchronic instantaneous water sampling survey both in springs and rain collectors would not be convincing as the two signals do not have relationship. To take into account drainage process, water sampled at spring has to be compared with an average signal of the rainfall event historic, weighted by rainfall event amount and event time from survey. This method involves, for an instantaneous spring water sampling, to have previously performed a campaign, at high sample rate resolution, of the rain collectors (ideally daily to weekly sample rate). However, this protocol is high time consuming and very expensive to implement. For this reason on Séchilienne, rain collectors had not taken instantaneous rain measurements. Instead, they were accumulated all rainfall event water between each water sampling campaign. Thus the isotopic signal was matching with the average rainfall signal on three months proportional to the rainfall amount. The same monitoring network as the one used for hydrochemistry and electrical conductivity was sampled for the isotope survey.

2.5. Hydrogeochemistry survey and electrical conductivity

Circulation of water in rock leached ions out of the geological formations. Water-rock interaction and relative mobility of ions are the prime factors influencing the geochemistry of the groundwater. Mineral phases dissolution is controlled by their dissolution rates, and the water-rock interaction time in the weathering zone, (Hilley et al., 2010). At Séchilienne, water spring chemistry depends mainly on (i) the contrasting lithology with the presence of sedimentary (carbonate rocks) and metamorphic (micaschists) formations,(ii) the pyrite alteration in the micaschist which promotes the alteration of other minerals (protons released) (Beaulieu et al., 2011, Li et al. 2008), (iii) the high solubility of carbonate minerals compared to silicate minerals (iiii) the degree of degradation of the rock between the stable and unstable zone leading to a modification of the minerals specific surface (Binet et al., 2007) and finally (iiiii) the dual- permeability of the metamorphic massif which can influence both the water-rock interaction time and the time variations of the chemical signal relatively to the recharge response (Pili et al., 2004).

Geochemistry of groundwater is discussed using major ions concentration. The nature and origin of the different springs is established by using a Durov diagram which allow to characterize the relationship between the different chemical facies (function of the lithology encountered) and their electrical conductivity (degree of mineralization). Major ions combinations were used to characterize water origin and flow path: Ca vs. HCO_3 for sedimentary cover and Na vs. Cl to discriminate precipitation or alteration of the micaschist (albite). In addition, the water content variations for each identified hydrochemical facies are investigated with Stiff diagrams. Finally, inverse modelling was performed on the springs chemical contents and rocks mineral phases using PHREEQC code (version 3.1.1, operating with the LLNL database) (Parkhurst and Appelo, 1999). This modelling allows (i) to characterize solid phases involved in the water-rock interaction process, (ii) to estimate the transfer of mass and (iii) to confirm flow path hypothesis from tracer tests and δO^{18}. Hydrochemical facies deduced from previous analysis have been then spatially mapped against geology. Additional measurements, performed in the G585 gallery by Vengeon (1998) in 1996 and in 1997 were also integrated in the hydrochemistry analysis. The gap with this study (2010-2012) is explained by (i) the crucial spatial interest of this gallery for the investigation as it is the only monitoring point located in the most active zone and (ii) the recent inaccessibility which did not allow to acquire new data. The low water period was determined from early June to late September, based on gross rainfall and effective rainfall analysis. Water chemistry seasonal variations are studied through the electrical conductivity, representative of the water total mineralization.

2.5.1. Contribution of site specific galleries

Natural and artificial tracers do not allow to characterize depth to the aquifer water level in this heterogeneous rock mass. However, on Séchilienne, absence of direct water pressure measurement can be compensated by galleries water inflows surveys which provide fundamental informations about depth of groundwater level within the unstable slope. At Séchilienne, three old mining galleries, situated at 900, 670 and 585 masl (G900, G670, G585), and a gallery dug to survey the landslide at 710 masl (G710) are located within the unstable area, with lengths of 60 m, 88m, 240m and 240m respectively (Fig. 1). All these galleries have a North-South orientation, except the G670 which is oriented N155, and intersect the unstable zone. Only the G585 is located in the most active zone of the landslide. Another gallery (GEDF), supplying the EdF hydropower plant (French Electricity company) is also located at the foot of the landslide slope at an elevation of about 425 masl. All these galleries have the particularity to show up bare rock, except the GEDF where some highly fractured zones were covered with concrete to support gallery against low rock competence. Finally, a piezometer is located near the G710 gallery but it only indicates water level from November 2009 to April 2010, as piezometer was clogged after that.

Fracturing and water inflows surveys were performed in theses galleries by Antoine (1993) and Vengeon (1998). A one-time hydrochemistry survey of water inflows was also performed in GEDF gallery in March 2002, complementary to the tracer-test. However, flow rates could not be evaluated and two qualitative attributes were assigned instead, leakage and abundant. A cross-section was designed to locate the water-level depth, based on a 3D model (geomodeler Gocad,(Mallet, 2002)). Depth extensions of faults and fractures were interpolated from geological map (Barféty et al., 1972) and fracturing mapping in galleries with variations of faults dips. Finally, depth delimitation of the unstable area was based on the geophysical survey performed by Le Roux et al. (2011).

2.6. Sample analysis

2.6.1. Survey of the tracer tests

Artificial tracers Uranin, Eosin, Rhodamin B and Sodium naphtionate) were extracted from charcoal adsorbents using an eluent (ethanol mixed with ammonia) which was then analyzed, such as the water samples collected manually and with automatic sampler, by a fluorescence spectrometer (Perkin-Elmer *LS 30* UV-Spectrometer Model). Accuracy depends on the natural organic matter content, which is highly variable through rainfall episodes

2.6.2. Oxygen stable isotopes

Water samples were collected in glass vials with cap that does not allow evaporation with an additional parafilm to prevent from any possible evaporation. Oxygen stable isotopes were analyzed with the Liquid Water Isotope Analyzers method (LWIA) using off-axis integrated cavity output spectroscopy analyzer (OA-ICOS), model DLT-100, manufactured by Los

Gatos Research Inc. For more details about method accuracy, precision and repeatability, see Penna et al. (2010) and Lis et al. (2008). Isotopic analyses were performed at the Faculty of Civil Engineering and Geosciences at the Delft University of Technology in the Netherlands.

2.6.3. Field measurement

The pH, electrical conductivity and temperature were measured on the field with a WTW apparatus model LF30 (a Xylem Inc. branch). pH and electrical conductivity probes were calibrated before each campaign with standard buffer solutions. Measurements are reduced to the standard temperature of 25 °C with a respective accuracy of 0.1 pH units and 0.1 µ S/cm.

2.6.4. Water chemistry analysis

Water samples were collected in polyethylene bottles and were filtered at 0.45µm. Action analyses of Na^+, Ca^{2+}, K^+, Mg^{2+} were performed by atomic absorption spectrometry (AA 100 Perkin–Elmer) with respective detection limits of 0.01; 0.5; 0.1 and 0.1 mg/L. Anion analyses of SO_4^{2-}, NO^{3-}, Cl^- were performed by high pressure ion chromatography (Dionex DX 100) with respective detection limits of 0.1; 0.05 and 0.1 mg/L. The concentrations in HCO_3^- were measured by acid titration with a N/50 H_2SO_4 acid few hours after sampling (maximum of 48 hours), with 1% accuracy. For the Séchilienne hydrochemical conditions (pH between 6 and 8.5), total and carbonate alkalinity can be considered as equivalent and equal to HCO_3^- ion concentration. The calculated charge balance error for the reported analyses was performed with the PHREEQC code (Parkhurst and Appelo, 1999). Only analyses which have a charge balance lower than 10% were taken into account. Silica was analyzed with a spectrophotometer (Spectroquant, Pharo 300, Merck) using silica-test kit (Merck) with 3% accuracy. Chemistry analyses were performed at the Chrono-Environnement laboratory at the University of Franche-Comté in France.

3. Results and discussion

3.1. Artificial tracing survey

3.1.1. Interpretation

In the Rochassier sinkhole test (Fig. 2A), one day after injection, Gallery 710 is reached by uranin, displaying a 3 km/day straight-line velocity. Numerous springs located on a limited area along the N20 Sabots fault (FON, MAT, BAT and NCH) have been tested positive, with velocities ranging from 0.45 to 0.84 km/day, as well as the exit of the gallery GEDF, (0.88 km/day). This test demonstrates the prominent role of the Sabots fault and GEDF gallery in the drainage of the slope. In addition, the velocity contrast between G710 and the other positive springs reveal that the drainage by the unstable slope bypasses the N20 faults, and is very likely performed by sub-surface drainage through a perched aquifer supported by a well-connected fractures network and involved a connection between sedimentary cover and unstable slope perched aquifer.

In the Mont-Sec crevasse test, two breakthroughs are displayed (Fig. 2B): G710 gallery and FON: (i) demonstrating: drainage conditioned by the unstable slope and the N70 fault direction, and (ii) corroborating the role of the N20 faults, respectively. Concerning velocities, a high difference can be observed between down slope flows (7-fold faster than lateral flows towards the N20 fault (0.55 *vs.* 0.08 km/day). This difference is attributable to: (i) the difference in hydraulic gradients alongside the steepest slope, and parallel to the elevation contour lines, and (ii) the widely open environment in the unstable zone.

The Gallery 900 test highlights a west main drainage component, except NCH and gallery G585, situated south-eastwards (Fig. 2C). This part of the unstable area, with a southwest drainage is very likely supported by the N70 high fracture network density and GEDF, whereas the southeast drainage seems to find the same origin as in previous tests, the major drainage role of the Sabots fault. The average speeds range between 0.06 and 0.16 Km/day.

The first test in the gallery 585 (G585- A test, Fig. 2D), with only surface springs monitored, has been detected at the GEDF gallery exit, confirming the role of GEDF in the interception of flow paths crossing the N70 discontinuities. Except the NCH spring (0.14 km/day), high speeds (0.49 to 2.36 km/day) are observed for the western springs.

The second G585 test (G585-B test, Fig. 2E), performed when the gallery GEDF was emptied, displays a breakthrough at four different kilometric points: 5.28 and 5.50 to the East, demonstrating the influence of the N20 Sabots fault, and 6.32 and 6.40 to the West, demonstrating the contribution of the N70 fractures.

Comparative analysis of the different tracer-tests allows characterizing better groundwater flow in the massif. GEDF exit shows high speeds (2.3 km/day) during G585-A test (Fig. 2D) and GEDF water inflows show low speeds (0.4 km/day) during G585-B test, but breakthrough times are similar (about one day). This velocity contrast is explained by the quasi-instantaneous transfer through the gallery GEDF, and groundwater speeds are in fact comparable. The same velocity range is observed for the eastern springs and for GEDF in the G900 and G585-A tests, about 0.15 and 2.3 km/day, respectively, reflecting that the eastern springs are partly recharged by water from the gallery GEDF.As a consequence, tracer velocities of the eastern springs are very likely overestimated by the GEDF gallery. Independently from the GEDF gallery, groundwater velocities though the unstable area for G900 and G585 tests can be estimated at 0.06 and 0.4 km/day respectively instead of 0.15 and 2.3 km/day.

Although G900 and G585-A tracer tests show common western breakthrough points, a high contrast of velocities is displayed (about 7 times higher for G585 test). This result can be explained by the injection location: G900 gallery injection point is indeed situated within the utmost unstable area whereas G585 gallery is situated in the most active unstable zone. This last zone, having a higher density of connected N70 discontinuities, promotes groundwater flow collected by the GEDF gallery. However, the Mont Sec crevasse test, also located on the utmost part, shows great velocities toward G710 (0.55 km/day) reflecting a high hydraulic gradient along the steepest slope and a very likely better organized medium.

Among the three tracer tests (Mont-Sec crevasse, G900, G585-A) a rather homogeneous speed (0.07 to 0.14 km/day) is observed for NCH and FON, both located along the N20 Sabots fault. These slow flows, compared to the one observed during the Rochassier test, demonstrate flow through micro-fissured block (more inertial) drained toward the east by N20 discontinuity. The Romanche River (ROM) is positive for two tracer tests (G900 and G585-A) meaning that the GEDF gallery collects only a part of the groundwater slope, the remaining reaching the River through the alluvium aquifer. Tracer velocities are also biased by the quasi-instantaneous transfer along the River, and groundwater velocity is estimated at 0.03 and 0.25 km/day, for the G900 and the G585-A tests, respectively.

The speeds estimated in this site range from 0.06 to 2.97 Km/day. The fastest ones, ranging from 0.4 to 2.97 km/d, (Rochassier, Mont Sec crevasse, and G585-B tests) display the same order of magnitude than in the Jura mountains karst systems (0.1 to 4 km/day, website of the Ministry of Environment), and far greater than other tracer tests performed in the basement rocks of Brittany (0.01 to 0.1 km/day, (Roques et al., 2014). Two factors, other than fracture aperture, can explain this velocity: (i) the widely open dense fracture network of the unstable media, promoting sub-surface perched drainage; (ii) the high general hydraulic gradient, parallel to the slope gradient.

3.1.2. Summary

The main insights obtained by these five tracer tests are a very likely perched sub-surface drainage draining water from the sedimentary cover toward the unstable slope with very rapid flow, promoted by widely open and connected media. The main N20 Sabots discontinuity plays a major role in the massif drainage, with rapid transfer, but drains also the unstable zone, with much slower velocities. This result highlights the dual permeability behaviour of fractured aquifer, with extended and widely open fractures vs. micro-fissured blocks. GEDF gallery is an open channel tunnel, and acts as a main drainage structure for the slope. It may regulate the piezometric surface, acting as a specified head boundary, collecting water from the up gradient slope, and re-distributing it down gradient in the aquifer. Remaining water not gathered by GEDF reaches the Romanche River.

3.2. Seasonal analysis

3.2.1. Isotope gradient

Fig. 3A shows gross and effective rainfall as well as actual evapotranspiration computed with method detailed in Vallet et al. (2013). Lysimeter shifting of isotopic gradient was only applied for the two last periods (Apr-Jun and Jul-Sep) where actual evaporation becomes really significant (Fig. 3B). Unfortunately, for the Jul-Sept period, no water was collected in the lysimeter. Although the slope was estimated with rain collectors, the lysimeter shift from the precedent period was used. Isotopic gradients have shown great variation according to the period having values of -0.12‰/100m, -0.25‰/100m, -0.21‰/100m and -0.18‰/100m, respectively, from first to last period (Fig. 3C). These values are conformed to commonly observed values ranging from -0.1‰ to -0.36‰ (Leibundgut et al., 2011).

3.2.2. Stable isotope analysis

Results from G710-1, which is a leakage point, collected with a 5m^2 cover, located at 70 m from the entrance of gallery 710, were not workable as they were given elevation either negative either inferior to collection point. This is probably due to an evaporation shift from gallery ambient temperature of air and water drop collection method (high air/water interaction). G710-2, which is also a leakage point of the gallery 710 collected in the same way, but is located 140 m far from the entrance, was not influenced by evaporation for the two first periods (lower temperature) but results were not exploitable for the two last periods. Deep snow make PLE spring unattainable for the first period (not sampled). Finally, DHU, COR, MTJ springs were dry for the last sampling period. It is worth mentioning that Romanche River and Rif Bruyant Stream were sampled only for the last period.

DHU and VIZ1 show the highest elevation compared to ridge line, respectively 157 and 139% (Fig. 4A and B). Although, their average recharge elevation is similar (about 1800 m), the seasonal variability is very distinct (STD of 32 and 315 m respectively for DHU and VIZ1). These two springs seem to be both influenced by massif slope groundwater and Romanche

River. DHU, located on the Romanche alluvium, seems to be more influenced by the inertial alluvial hydrosystem which buffers the isotopic water signal from the massif. On the contrary, recharge area of VIZ1, located at the foot of the slope, is more reactive to seasonal conditions, with influenced related to Romanche River increasing from low to high water period, meaning that during high recharge season the spring is mainly recharged by the slope. It is not physically possible that VIZ1 be recharged by alluvial aquifer, so the only explanation is that the open EDF gallery, which withdraws water from the Romanche, recharges the slope aquifer on its western part.

COR, MOU, CMJ, MTJ, and PLE show mean elevation of recharge area close to their associated ridge points (maximum of 4% higher), with a very low seasonal dispersion (no significant difference from one season to another) meaning that recharge area is local and relatively insensitive to aquifer saturation level (except MOU which has a greater variability) (Fig. 4A and B). This inertia can be explained by a water supply essentially from interstices/cracks capacitive rock reservoir. G710-2 has only been sampled twice, and it is not possible to assess clearly the seasonal variation. However, springs recharge area seems mainly local as the two high water period survey show a mean recharge area relatively low compared to the behaviour of the massif springs.

On the contrary, BAT, THL, THE, MAT, and FON show a mean elevation clearly higher than elevation of associated ridge point (16% higher on average) and a variability far greater (average STD of 100 m) (Fig. 4A and B). Apart from FON, these springs show the same seasonal variation having remote recharge area location (elevation increase) gradually that season from high water level to dry season. This reactivity and behaviour are typical of springs supplied by fractured drainage of the aquifer, mechanism accentuated during low water period. It is worth mentioning that VIZ1 shows the same seasonal pattern meaning that this spring is probably also supplied by network of discontinuities. To a lesser extent, AIL show as well a remote recharge area (9% higher) with moderate variability and no clear seasonal pattern.

CBE has two extreme points during spring and summer, which are probably the consequences of significant contributions from accumulated ^{18}O depleted winter precipitation to ground water recharge. This mechanism involves a long residence time, demonstrating a likely rock micro-fissured blocks supply. Mean recharge area and STD were then only estimated with the two high water periods. Along, MOU, AIL and FON show high elevation recharge area for the first season (Nov-Dec), even above the highest massif peak (Pic Oeilly) (Fig. 4A and B). These high recharge elevation points can be explained partly by uncertainties of the method and also by water anomalies depleted in ^{18}O, compared to content in precipitation (rainfall +snow melt). This can find origin from combination of recharge area micro-scale effect (wind and solar exposure for example) and complex changes in isotopic content which occur between snow accumulation and melt (Cooper, 1998). These aberrant values were disregarded to estimate the mean elevation average and the standard deviation (STD).

3.2.3. Electrical conductivity

DHU and VIZ1 springs show low electrical conductivity (about 340 μS/cm) with similar variability (STD about 14) (Fig. 4C). Romanche electrical conductivity is lower (200 μS/cm) but GEDF water inflows have shown up values up to 1500 μS/cm, meaning that water from GEDF have probably a higher value than the Romanche. Low variability of VIZ1 (contrary to recharge elevation) reflects the water mixing from slope aquifer and GEDF water, of which water mineralization difference has a greatest amplitude on low water period season (high values buffered).

COR, MTJ, CBE, PLE show low to moderate variability as well as no clear seasonal pattern meaning that water flow of theses springs is mainly controlled by the aquifer micro-fissured blocks component having an inertial behaviour and relatively insensitive to seasonal variation (Fig. 4C). PLE has very low conductivity probably due to low water-rock interaction time but 18O signal is relatively scattered. One possible explanation is that this spring is recharge by rapid water flow through sedimentary cover. MOU and AIL mineralization are very insensitive to seasonal variation (STD of 5) and have low electrical conductivity values. MOU and AIL behaviour is probably due to the recharge of the slope aquifer by the Rif Bruyant Stream, having an electrical conductivity of 150µS/cm, which smoothes over the signal (similar as VIZ1). MOU being less impacted thanks to its remote location from the stream. This dilution by surface network (1010 masl ^{18}O recharge area elevation) has certainly drawn to the bottom the estimated recharge area elevation of the slope aquifer water recharging the springs. This influence of Rif Bruyant explained also why MOU has a scattered distribution of recharge area elevation (Fig. 4A and B) with a mean recharge elevation below associated ridge line point (contrary to COR, MTJ, CBE).

CMJ, BAT, THL, THE, MAT, FON show high variability (STD of 22 on average) very sensitive to seasonal variation, having the lowest value observed during the high water period and inversely for lowest values (Fig. 4C). These springs are very sensitive to seasonal variation providing evidence of rapid water flow in fissures during high water period (dilution) and drainage of the micro-fissured blocks during low water period (interaction water-rock). THE show low electrical conductivity compared to the others springs but variability is similar, probably due to different groundwater flow path. G710-2 show the highest water mineralization and seasonal variability consequence of groundwater flowing in the unstable, widely open and transmissive, with constant opening and closing of fissures, which modify the water-rock interaction (Binet et al., 2009).

3.2.4. Summary

Two main recharge types were identified, rapid and reactive water flow in fissures (CMJ, BAT, THL, THE, MAT, FON, AIL, MOU, VIZ1) bypassing the bulk of the less pervious and inertial cracks/interstice of which COR, CMJ, and MTJ are dependent. Among these main hydrodynamic behaviours, several springs are locally influenced. CMJ is the only spring recharged by fractured network which has a local recharge area whereas the others show remote location. CBE show probably an intermediate recharge mechanism partly by fractured network and partly by micro-fissured blocks. VIZ1 and MOU -AIL are influenced by surface water, the Romanche (by the intermediary of GEDF gallery) and the Rif Bruyant respectively. Then MOU and AIL have a very likely higher mean recharge area elevation. G710-2 behaviour stands out from the massif springs and it is clearly marked by the unstable slope destabilisation and open medium. Finally, PLE and DHU have specific functioning, respectively “karstic” and alluvial.

Looking at the geological structures, it seems obvious that the two major discontinuities striking N20 (Sabots and Séchilienne faults) play a crucial role in the massif drainage as well as the East-West GEDF gallery (Fig. 4D, interpreted). These local high hydraulic conductivity objects are contrasted by a more inertial aquifer (reservoir function of cracks/interstices) bearing them. Only one point in the unstable area indicates that water origin is mainly local, crossing a widely open and permeable medium.

3.3. Low water survey: hydrochemistry

3.3.1. Hydrochemical groups

The percentage distribution of major cations and anions in the Durov diagram highlights 4 distinct water chemistry groups reflecting groundwater flow through different geological settings (Fig. 5A, Tab. 1). The first group corresponds to Ca-HCO_3-rich water (PLE) with low of electrical conductivity (about 100 µS/cm). The second group corresponds to Mg-Ca-HCO_3-rich water (AIL, MOU, MTJ, CMJ and COR) where Ca and Mg are in the same proportions. Electrical conductivity increases from the springs AIL (202 µS/cm) and MOU (367 µS/cm), with intermediate values for CMJ (440 µS/cm) and MTJ (455 µS/cm) springs, to reach values of about 540 µS /cm for the COR spring. Water composition of the third group varies from Mg-Ca-HCO_3-SO_4-rich water (G585-2 and G585-3), with intermediate Mg-Ca-SO_4-HCO_3-rich water (G585-1 and G710-2), to Mg-Ca-SO_4-rich water (G710-1). G585-2 and G585-3 are characterized by electrical conductivity values between 320 and 446 µS/cm. Water from G585-1 and G710-2 has higher values of electrical conductivity (respectively 630 and 870 µS/cm) than water from G710-1 (385 µS/cm). The group 4 corresponds to Ca-Mg-HCO_3-SO_4-rich water (VIZ1, THE, THL, CBE, BAT, MAT and FON). VIZ1 and THE have similar values of electrical conductivity (respectively 350 and 330 µS/cm). The THL and CLE springs have higher values than the previous ones (about 470 µS/cm) but there are lower than BAT, MAT and FON springs (520 µS/cm).

3.3.2. Mineralization origin

The alteration of each of the three distinct lithologies (moraine, carbonate rock and micaschist) products ions which may be common to more than one geological formation. Indeed, Ca may result from calcite dissolution, present both in the sedimentary cover and in the calcite veins of the basement. Mg can originate from dolomite but also from minerals of the basement (chlorite, phengite and phlogopite). HCO_3 is mainly associated with the dissolution of calcite and dolomite, and to a lesser extent to silicate weathering (albite, muscovite). However, apart from the calcite, it is possible to discriminate the lithological origin of ions thanks to the difference of solubility of the dissolved minerals. On the contrary, Na and SO_4 are clearly identified as markers of the micaschist basement. Na, in excess with respect to Cl, originates from silicates dissolution (albite). The δS^{34} analyzes, performed by Vengeon (1998), show that SO_4 has a sulfurized origin, due to alteration of pyrite, present only in the basement (very soluble mineral in the presence of oxygen). This alteration releases protons (Equ. 1) which can consume afterwards the HCO_3, produced by the dissolution of carbonate minerals (Equ. 2), releasing CO_2 and H_2O (Equ. 3).

$$FeS_2 + \frac{15}{4} * O_2 + \frac{7}{2} * H_2O \leftrightarrow Fe(OH)_3 + 2SO_4^{2-} + 4H^+ \quad (1)$$

$$(Ca, Mg)(CO_3)_2 + 2H_2O + 2CO_2 \leftrightarrow Ca^{2+} + Mg^{2+} + 4HCO_3^- \quad (2)$$

$$HCO_3^- + H^+ \leftrightarrow H_2O + CO_2 \quad (3)$$

This succession of chemical reaction explains the range of pH (between 7 and 8) measured in the Séchilienne water despite the production of protons (Tab.1) and results in depletion of HCO_3 ions with respect to Ca and Mg, the latter becoming balanced by SO_4. The oxidation of pyrite leads to the deposition of a layer of iron hydroxide on its surface which mitigates its alteration over time (decrease of the reactive surface).

Inverse modelling is performed to investigate the minerals assemblage which has driven to the chemistry composition of the Séchilienne identified hydrochemical facies. Inverse modelling allows to calculate mass transfers of water-rock interaction (dissolve, precipitate and degas) which explain the difference in composition between initial and final water. Initial water matches with an average composition of rainwater falling in the Alps (Atteia, 1994). Minerals representative of the sedimentary cover and micaschist bedrock were chosen according to Vengeon geological survey (1998) (Tab.2).

3.3.3. Mineralization interpretation

The hydrochemistry analysis has identified four chemical facies which are spatially constrained with respect to Séchilienne landslide and geological structures. (Fig. 5D). Springs of group 1 (PLE) and 2 (AIL, MOU, MTJ, CMJ, COR) are representative of the flow in the stable area with no possible influence of transit through the unstable area. Points of the group 3 (G585-1, G585-2, G585-3, G710-1, G710-2), all situated in the instability, have chemistry representative of the water-rock interaction in the unstable area. Finally, the springs of group 4 (THE, THL, CBE, BAT, MAT and FON) are located along the Sabots fault of which artificial tracer tests (Rochassier and G900) show a double origin of the water, mixture of the sedimentary cover and the unstable area.

Stable area (Group 1 and 2)

The group 1 (PLE) has a Ca-HCO_3 facies. The low concentrations of Ca and HCO_3 of this group, located on the calcite equilibrium line, is representative of water circulating in a carbonate or calcite dominant cover (limestone or moraines) with a short residence time (Fig. 5B). For group 2, the inverse model calculation was made only for springs of MTJ, CMJ, and COR, as concentrations of AIL and MOU springs, although in the same proportions, are diluted by the Rif Bruyant Stream (seasonal analysis). Inverse modelling results show that the Mg concentrations come from 90% of dolomite and 10% of the phlogopite. 87% of the Ca is derived from the dolomite and the remaining 14% from the calcite. Therefore the high Mg concentrations are explained by water transit through the sedimentary cover. However, these springs composition is above the dolomite equilibrium line (Fig. 5B) which is explained by a consumption of HCO_3 by protons produced by the alteration of the pyrite. The difference in mineralization between MTJ, CMJ and COR results from increasing residence time in the basement, as demonstrated by the increasing concentrations of Na and SO_4 from MTJ to COR (Fig. 5C).

Unstable area (Group 3)

For group 3, the calculation of inverse model was made only for G710-2 because this point has the higher mineralization, indicator of a water flowpath in a high altered environment, considered then as marker of the unstable area. The Mg concentrations come from 37% of the dolomite and 63% of the chlorite (phlogopite alteration) 42% of the Ca is derived from the dissolution of the dolomite and the remaining 58% of the calcite. In addition, this group is characterized by the highest concentrations of SO_4 (Tab.1) which can be explained by two mechanisms related to the deformation of the slope. First of all, the opening and/or closing of fractures and cracks leading to new flowpath through unaltered pyrites zones (Calmels et al,

2007) and secondly the friction and grinding along fractures due to the movement of rock masses which cause a refreshment of pyrite reactive surface increasing the weathering rate (Binet et al. 2009). Finally, the alteration of the pyrite promotes alteration of veins of carbonates and silicates (Dongarrà et al., 2009; Gaillardet et al., 1999), as shown by the high concentrations of Ca in G710-2 (Fig. 5B) and Na in the G710 gallery (Na has not been analyzed for G585 water inflows) (Fig. 5C). The acquisition of mineralization occurs largely with the interaction of the basement minerals and SO_4 is without doubt the marker of the unstable area. Difference of the mineralization among the different gallery points is due to the unstable area heterogeneity of distribution of minerals within the basement and fracture network.

Mixing area (Group 4)

The VIZ1, THE, THL, CBE, BAT, MAT and FON, springs clearly denote from other springs by concentrations of Ca, Na and SO_4. The Ca concentrations are nearby the calcite equilibrium line (Fig. 5B) reflecting a transit on the limestone and/or moraine, which is consistent with the results of δO^{18}. Transit in the stable bedrock area cannot explain the SO_4 concentrations which are up to 25% higher than the springs of the stable area (group 2) and 75% lower than the waters of the unstable area (group 3). Mixing test was performed with water of carboniferous pole (PLE) and with water of the unstable area (G710-2) to quantify the contribution of each component (sedimentary cover and unstable area). Water composition of group 3 is explained by a mixture corresponding to a water inflow of 30% of the unstable area and 70% of the sedimentary cover consistent with δO^{18} results. However, the mixing computation requires four times more mineralized water than PLE water, meaning that the carbonate component of the mixture has a longer residence time in the sedimentary cover. Finally, VIZ1 is also a water mixture but from the Romanche River, the stable area and the unstable zone through the drainage of the GEDF gallery.

3.3.4. Summary

Three different origins have been highlighted in the area of Séchilienne: stable area, unstable area and mixing area. Springs of the stable area are influenced by calcite sediment cover for group 1 and by dolomite cover and basement for group 2. In the unstable zone, although water originates partly from sedimentary cover, the mechanical weathering is the dominant factor of the water mineralization supplanting the variations of residence time, of which SO4 is the marker. Finally, the springs located along the Sabots fault (Group 3) are explained by a mixture of carbonate (limestone or moraine) and bedrock component promoted by the fault drainage properties. The springs of AIL, MOU and VIZ1 are also influenced by surface water, the latter having a more complex signal due to the influence of the GEDF gallery.

3.4. Contribution of galleries

3.4.1. Unstable area

The highest gallery (G900) is always dry and no water inflows have been identified. G710 gallery shows, weak but quasi-permanent, two leakage zones at 80 m and 150 m from entrance (respectively G710-1 and G710-2). Two leakage zones have also been identified for the G670 gallery at 25m and 70m of the gallery entrance (CETE, 2006). Water inflows in the G585 gallery are more numerous and abundant than the three previous galleries with temporary (202 m, G585-3) and permanent water inflow (160 m, G585-1) and a localized leakage area (170 m, G585-2). G585-1 water inflow probably corresponds to a rapid flow from surface (Vengeon, 1998). Galleries water inflows are localized on fracture damaged zone (Fig. 6C) reinforcing the prominent role of fractures network in the groundwater flow path bypassing the less pervious matrix. Before the piezometer was clogged, water level fluctuations have been recorded between 590 and 602 masl during four months, from end of November 2009 to beginning of April 2010 (Fig. 6B). The piezometric level was measured in high water period, thus it is very likely that it indicates the maximum level that the groundwater can reach. This is especially true given that cumulated precipitation on this period is about 445 mm which is far higher than an average year (330 mm from 1992 to 2012).

3.4.2. GEDF Gallery

The GEDF gallery has the particularity to show up bare rock and to have water which circulates freely by gravity from Romanche collecting point to Vizille hydropower plant (contrary of a hermetic pressure pipe). During the excavation of the GEDF gallery, perennial springs located at Les Rivoirands and at Chamoussière village were permanently dried up (Fig. 6A). Additionally to water inflow surveys, cemented part (maintain the gallery wall) of the GEDF gallery indicated unstructured zone and very likely water inflows. Numerous and scattered water inflows and leakages are occurring in the GEDF gallery between 5.5km and 7 km, matching with a dense network of local fractures consequences of the destabilization (Fig. 6A). Numerous water inflows have been also observed on the western part, between 7 and 7.5 km (apparent absence of fractures is due to absence of survey but cemented parts confirm their presence). On the contrary, at the East of the landslide discontinuities density is low but faults/fractures are major with greater spatial extension. Water inflows are better spatially constrained, localized on the discontinuities, and qualified of abundant. Between 3.9km and 4.5km, the Séchilienne fault has completely unstructured the zone and many water inflows occurred, revealing its prominent drainage role. To a lesser extent, the Sabots fault seems to have a more localized impact on the GEDF gallery water inflows. Hydrochemistry survey shows that SO_4 is the marker of the unstable slope having the highest value (Chapter 3.3). Average SO_4 concentration of COR and G710-2 during high water period, representative of groundwater flow in the stable and unstable zones respectively, are plotted relatively to SO_4 concentration measured in the water inflow from GEDF gallery. From kilometric point 4 to 5.80, SO_4 signal is similar to COR whereas from 6 to 7 kilometric points SO_4 signal increases and even largely exceeds the concentration of G710-2. SO_4 signal confirms the prominent unstable slope drainage role of the GEDF gallery.

3.4.3. Summary

Water inflows survey of the four galleries located in the unstable area highlight that the quasi-permanent water inflows or leakages are supported by fractures damaged zone. Unstable area bears a very likely perched aquifer supported by the dense and well-connected fractures network (Rochassier and G90 tracer tests). The latter compartments the unstable area into less transmissive zone. The piezometer and the gallery G585 reach the deep aquifer, outside of the unstable area, and are very likely located in the top part of the water-level fluctuation zone (no permanent flow or water-level). GEDF gallery acts as a major drain in the massif, and especially in front of the unstable area where the high density fracture network accentuates the drainage, and imposes a constant head which very likely constrains the groundwater level at gallery elevation (about 425 masl). A steepest slope hydraulic gradient of 80 m/100m has been estimated between the piezometer and GEDF gallery. In addition, an average position of the deep aquifer water-level within the slope with possible fluctuations zones have been estimated along the North-South cross-section XY (Fig. 6C), using projected galleries and piezometer hydrogeology data.

3.5. Groundwater conceptual model

Discontinuities: major drain

The two N20 faults (Sabots and Séchilienne) act as major drainage axis of the massif. For Séchilienne fault damaged zone even promote water infiltration from surface water (Rif Bruyant) upstream of AIL springs (Fig. 7A). The Sabots fault seems to drain out most of the sedimentary cover perched aquifer. Additionally, this discontinuity has a significant spatial influence draining out the deep aquifer below unstable slope, likely due to a lowering of groundwater level, which causes a West to East hydraulic gradient perpendicular to the fault. Tracer-test speeds, δO^{18}.and water mixing indicate that this drainage is done through the micro-fissured blocks aquifer component and is minor relatively to Sabots fault drainage axis. Outside of the major discontinuities, the groundwater behaviour is more inertial, having a longer residence time reflected by springs of the northern slope of the Mont Sec massif.

Unstable area: sub-surface drainage

The unstable slope extension acts as a sub-surface high hydraulic conductivity perched aquifer sustained by the dense N70 fractures network, which divided up the unstable slope into less transmissive compartments. Although the G710 gallery drains out mainly local water (stable isotope), a non-negligible part originated from rapid transfer from the sedimentary cover perched aquifer (tracer-tests), involving a sub-surface drainage supported by a well connected fractures network by passing the deep aquifer flow. This recharge mechanism is only possible by the intermediary of a hydraulic connection between unstable slope and sedimentary perched aquifer leading to a continuous sub-surface drainage (Fig. 7A).

Unstable area: deep aquifer

Water from disorganized unstable slope, having high infiltration rates, flows toward the deep aquifer, located about 100 m below, through the dense N70 discontinuities network. The GEDF gallery operates as major East-West massif drain of which the rate and the effect are controlled by the N70 crossing discontinuities density and aperture. Groundwater which is not collected by GEDF likely flows toward the Romanche alluvium aquifer. As a consequence, deep aquifer water-level is subjugated by the constant water head of GEDF and Romanche alluvium. In addition, GEDF gallery on its eastern part recharges the massif deep aquifer with mixed water from the Romanche River and water inflow.

Relationship groundwater - unstable slope destabilisation

Although Séchilienne deep seated landslide destabilization is mainly controlled by rain triggering (short term component), time-dependent factors (long term component) such as rock weakening and modification of unstable slope hydraulic field stress are significant. Indeed, long term displacement monitoring, shows that displacement rate and amplitude have significantly increased with time (materialise by the trend), independently of the recharge amount, consequences of a progressive deterioration of rock mechanical properties (Fig. 7B). Detrended time series which is clearly linked to the hydrocyle (Vallet et al., 2013), can be decomposed into an irregular and seasonal component, which may be associated to unstable slope perched and deep aquifer water-level fluctuations, respectively. Indeed, perched aquifer behaviour is more reactive to rainfall events with limited pore pressure building (high infiltration rate) whereas deep aquifer is more sensitive to seasonal recharge variations. The signal similarity between irregular component and gross rainfall, and seasonal component and effective rainfall (Fig. 7B) support this hypothesis. This signal analysis show the very likely dual-influence of the two identified hydrosystems, sub-surface and deep, on the unstable slope of which deep aquifer impact has been recently confirmed by Cappa et al. (2014).

4. Conclusion

This survey highlights the dual-permeability properties of fractured rock aquifer and also the dual-rock properties due to disorganized and widely open unstable area relatively to intact rock mass outside of the landslide. This heterogeneity drives to a dual hydrosystem, with sub-surface perched aquifers drainage localized in the unstable area (and for Séchilienne site in the sedimentary cover) and a deep aquifer on the whole massif bearing the landslide, both impacting the destabilisation. Seasonal monitoring of natural and artificial tracers has allowed to characterize the groundwater scheme surrounding the unstable slope and to refine and better constraining the Séchilienne unstable slope conceptual model. Method developed for study has allowed to well constrain the groundwater flow scheme despite the sparse data context. Results of this study have already been used to perform an advanced hydromechanical study (Cappa et al., 2014). Forthcoming of this research is a quantitative signal analysis using cross-wavelet and time series decomposition. A lump modelling is also planned to better characterize the dual-hydrosystem functioning and its impact on the Séchilienne landslide destabilisation rate.

Acknowledgments

This research was fund by the program SLAMS (Séchilienne Land movement: Multidisciplinary Studies) of the Agence Nationale de la Recherche. The meteorological and displacement data were supplied by CETE Lyon. The authors gratefully acknowledge the support of Jean-Pierre Duranthon and Marie-Aurélie Chanut from the CETE Lyon. Implementation of the monitoring network would not have been possible without the cooperation of Mrs. and Mr. Aymoz, Patrick Boyer from the Office National des Forêts and the mayor of Séchilienne Gérard Cret.

References

Alfonsi, P.: Relation entre les paramètres hydrologiques et la vitesse dans les glissements de terrains. Exemples de La Clapière et de Séchilienne, Revue française de géotechnique, (79), 3–12, 1997.

Antoine, P.: Visite de la galerie EDF., 1993.

Van Asch, T. W. ., Buma, J. and Van Beek, L. P. .: A view on some hydrological triggering systems in landslides, Geomorphology, 30(1–2), 25–32, doi:10.1016/S0169-555X(99)00042-2, 1999.

Atteia, O.: Major and trace elements in precipitation on Western Switzerland, Atmospheric Environment, 28(22), 3617–3624, doi:10.1016/1352-2310(94)00193-O, 1994.

Bakalowicz, M.: Contribution de la géochimie des eaux à la connaissance de l'aquifère karstique et de la karstification, PhD thesis, University Pierre et Marie Curie, Paris VI, Paris., 1979.

Barféty, J.-C., Bordet, P., Carme, J., Debelmas, J., Meloux, M., Montjuvent, G., Mouterde, R. and Sarrotreynauld, J.: Carte géologique détaillée de la France,, 1972.

Belle, P., Aunay, B., Bernardie, S., Grandjean, G., Ladouche, B., Mazué, R. and Join, J.-L.: The application of an innovative inverse model for understanding and predicting landslide movements (Salazie cirque landslides, Reunion Island), Landslides, 1–13, doi:10.1007/s10346-013-0393-5, 2013.

Binet, S.: L'hydrochimie, marqueur de l'évolution à long terme des versants montagneux fracturés vers de grands mouvements de terrain Application à plusieurs échelles sur la haute vallée de la Tinée (Mercantour, France) et sur le versant de Rosone (Gran Paradiso, Italie), PhD thesis, Université de Franche-Comté, Besançon, 10 March. [online] Available from: http://tel.archives-ouvertes.fr/tel-00090307, 2006.

Binet, S., Guglielmi, Y., Bertrandet, C. and Mudry, J.: Unstable rock slope hydrogeology: insights from the large-scale study of western Argentera-Mercantour hillslopes (South-East France), Bulletin de la Societe Geologique de France, 178(2), 159–168, doi:10.2113/gssgfbull.178.2.159, 2007.

Binet, S., Spadini, L., Bertrand, C., Guglielmi, Y., Mudry, J. and Scavia, C.: Variability of the groundwater sulfate concentration in fractured rock slopes: a tool to identify active unstable areas, Hydrol. Earth Syst. Sci., 13(12), 2315–2327, doi:10.5194/hess-13-2315-2009, 2009.

Bogaard, T., Guglielmi, Y., Marc, V., Emblanch, C., Bertrand, C. and Mudry, J.: Hydrogeochemistry in landslide research: a review, Bulletin de la Societe Geologique de France, 178(2), 113–126, doi:10.2113/gssgfbull.178.2.113, 2007.

Bonzanigo, L., Eberhardt, E. and Loew, S.: Hydromechanical factors controlling the creeping Campo Vallemaggia landslide, in Symposium of landslides, Causes, Impacts and Countermeasures, pp. 13–22, UEF, Davos, Switzerland., 2001.

Cappa, F., Guglielmi, Y., Rutqvist, J., Tsang, C.-F. and Thoraval, A.: Hydromechanical modelling of pulse tests that measure fluid pressure and fracture normal displacement at the

Coaraze Laboratory site, France, International Journal of Rock Mechanics and Mining Sciences, 43(7), 1062–1082, doi:10.1016/j.ijrmms.2006.03.006, 2006.

Cappa, F., Guglielmi, Y., Soukatchoff, V. M., Mudry, J., Bertrand, C. and Charmoille, A.: Hydromechanical modeling of a large moving rock slope inferred from slope levelling coupled to spring long-term hydrochemical monitoring: example of the La Clapière landslide (Southern Alps, France), Journal of Hydrology, 291(1–2), 67–90, doi:10.1016/j.jhydrol.2003.12.013, 2004.

Cappa, F., Guglielmi, Y., Viseur, S. and Garambois, S.: Deep fluids can facilitate rupture of slow-moving giant landslides as a result of stress transfer and frictional weakening, Geophysical Research Letters, n/a–n/a, doi:10.1002/2013GL058566, 2014.

Cervi, F., Ronchetti, F., Martinelli, G., Bogaard, T. A. and Corsini, A.: Origin and assessment of deep groundwater inflow in the Ca' Lita landslide using hydrochemistry and in situ monitoring, Hydrol. Earth Syst. Sci., 16(11), 4205–4221, doi:10.5194/hess-16-4205-2012, 2012.

Chanut, M.-A., Vallet, A., Dubois, L. and Duranthon, J.-P.: Mouvement de versant de Séchilienne : relations entre déplacements de surface et précipitations – analyse statistique, in Journées Aléa Gravitaire 2013, Grenoble, France., 2013.

Clark, I. D. and Fritz, P.: Environmental Isotopes in Hydrogeology, CRC Press., 1997.

Clauser, C.: Permeability of crystalline rocks, Eos, Transactions American Geophysical Union, 73(21), 233–238, doi:10.1029/91EO00190, 1992.

Cooper, L. W.: Chapter 4 - Isotopic Fractionation in Snow Cover, in Isotope Tracers in Catchment Hydrology, edited by C. KENDALL and J. J. McDONNELL, pp. 119–136, Elsevier, Amsterdam., 1998.

Corominas, J., Moya, J., Ledesma, A., Lloret, A. and Gili, J. A.: Prediction of ground displacements and velocities from groundwater level changes at the Vallcebre landslide (Eastern Pyrenees, Spain), Landslides, 2(2), 83–96, doi:10.1007/s10346-005-0049-1, 2005.

Dongarrà, G., Manno, E., Sabatino, G. and Varrica, D.: Geochemical characteristics of waters in mineralised area of Peloritani Mountains (Sicily, Italy), Applied Geochemistry, 24(5), 900–914, doi:10.1016/j.apgeochem.2009.02.002, 2009.

Gaillardet, J., Dupré, B., Louvat, P. and Allègre, C. J.: Global silicate weathering and CO2 consumption rates deduced from the chemistry of large rivers, Chemical Geology, 159(1–4), 3–30, doi:10.1016/S0009-2541(99)00031-5, 1999.

Gat, J. R.: Oxygen and Hydrogen Isotopes in the Hydrologic Cycle, Annual Review of Earth and Planetary Sciences, 24(1), 225–262, doi:10.1146/annurev.earth.24.1.225, 1996.

Grasso, J.-R., Tatard, L., Voisin, C., Sue, C. and Sira, C.: Assessment of earthquake triggering potency for landslides, French Alps : interactions between strong topography contrast, low tectonic loading, and low weathering context, in JAG 2013, Grenoble, France. [online] Available from: http://isterre.fr/recherche/equipes/risques/actualites/autres-evenements/journees-alea-gravitaire-17-18/presentations/article/assessment-of-earthquake (Accessed 30 October 2013), 2013.

Guglielmi, Y., Cappa, F. and Binet, S.: Coupling between hydrogeology and deformation of mountainous rock slopes: Insights from La Clapière area (Southern Alps, France), Comptes Rendus Geoscience, 337(13), 1154–1163, doi:10.1016/j.crte.2005.04.016, 2005.

Guglielmi, Y., Vengeon, J. M., Bertrand, C., Mudry, J., Follacci, J. P. and Giraud, A.: Hydrogeochemistry: an investigation tool to evaluate infiltration into large moving rock masses (case study of La Clapière and Séchilienne alpine landslides), Bulletin of Engineering Geology and the Environment, 61(4), 311 – 324, 2002.

Helmstetter, A. and Garambois, S.: Seismic monitoring of Séchilienne rockslide (French Alps): Analysis of seismic signals and their correlation with rainfalls, J. Geophys. Res., 115(F3), F03016, doi:10.1029/2009JF001532, 2010.

Hilley, G. E., Chamberlain, C. P., Moon, S., Porder, S. and Willett, S. D.: Competition between erosion and reaction kinetics in controlling silicate-weathering rates, Earth and Planetary Science Letters, 293(1–2), 191–199, doi:10.1016/j.epsl.2010.01.008, 2010.

Hong, Y., Hiura, H., Shino, K., Sassa, K., Suemine, A., Fukuoka, H. and Wang, G.: The influence of intense rainfall on the activity of large-scale crystalline schist landslides in Shikoku Island, Japan, Landslides, 2(2), 97–105, doi:10.1007/s10346-004-0043-z, 2005.

Iverson, R. M.: Landslide triggering by rain infiltration, Water Resources Research, 36(7), 1897–1910, doi:10.1029/2000WR900090, 2000.

Leibundgut, C., Maloszewski, P. and Külls, C.: Tracers in Hydrology, John Wiley & Sons., 2011.

Lis, G., Wassenaar, L. I. and Hendry, M. J.: High-Precision Laser Spectroscopy D/H and 18O/16O Measurements of Microliter Natural Water Samples, Anal. Chem., 80(1), 287–293, doi:10.1021/ac701716q, 2008.

Mallet, J.-L.: Geomodeling, Oxford University Press, Oxford; New York., 2002.

Maréchal, J.-C. and Etcheverry, D.: The use of 3H and delta18O tracers to characterize water inflows in Alpine tunnels, Applied Geochemistry, 18(3), 339–351, 2003.

Mudry, J.: Apport du traçage physico-chimique naturel à la connaissance hydrocinématique des aquifères carbonatés, PhD thesis, Université de Franche-Comté, Besançon, 5 May. [online] Available from: http://tel.archives-ouvertes.fr/tel-00654518 (Accessed 30 January 2014), 1987.

Parkhurst, D. L. and Appelo, C. A. J.: User's guide to PHREEQC (Version 2): A computer program for speciation, batch-reaction, one-dimensional transport, and inverse geochemical calculations,, 1999.

Penna, D., Stenni, B., Šanda, M., Wrede, S., Bogaard, T. A., Gobbi, A., Borga, M., Fischer, B. M. C., Bonazza, M. and Chárová, Z.: On the reproducibility and repeatability of laser absorption spectroscopy measurements for δ2H and δ18O isotopic analysis, Hydrol. Earth Syst. Sci., 14(8), 1551–1566, doi:10.5194/hess-14-1551-2010, 2010.

Pili, É., Perrier, F. and Richon, P.: Dual porosity mechanism for transient groundwater and gas anomalies induced by external forcing, Earth and Planetary Science Letters, 227(3–4), 473–480, doi:10.1016/j.epsl.2004.07.043, 2004.

Rochet, L., Giraud, A., Antoine, P. and Évrard, H.: La déformation du versant sud du mont-sec dans le secteur des ruines de Séchilienne (Isère), Bulletin of the International Association of Engineering Geology, 50(1), 75–87, doi:10.1007/BF02594959, 1994.

Ronchetti, F., Borgatti, L., Cervi, F. and Corsini, A.: Hydro-mechanical features of landslide reactivation in weak clayey rock masses, Bull Eng Geol Environ, 69(2), 267–274, doi:10.1007/s10064-009-0249-3, 2010.

Roques, C., Bour, O., Aquilina, L., Dewandel, B., Leray, S., Schroetter, J., Longuevergne, L., Le Borgne, T., Hochreutener, R., Labasque, T., Lavenant, N., Vergnaud-Ayraud, V. and Mougin, B.: Hydrological behavior of a deep sub-vertical fault in crystalline basement and relationships with surrounding reservoirs, Journal of Hydrology, 509, 42–54, doi:10.1016/j.jhydrol.2013.11.023, 2014.

Le Roux, O., Jongmans, D., Kasperski, J., Schwartz, S., Potherat, P., Lebrouc, V., Lagabrielle, R. and Meric, O.: Deep geophysical investigation of the large Séchilienne landslide (Western Alps, France) and calibration with geological data, Engineering Geology, 120(1–4), 18–31, doi:10.1016/j.enggeo.2011.03.004, 2011.

Rutqvist, J. and Stephansson, O.: The role of hydromechanical coupling in fractured rock engineering, Hydrogeology Journal, 11(1), 7–40, doi:10.1007/s10040-002-0241-5, 2003.

Sun, J., Liu, Q., Li, J. and An, Y.: Effects of rainfall infiltration on deep slope failure, Science in China Series G: Physics Mechanics and Astronomy, 52(1), 108–114, doi:10.1007/s11433-009-0004-6, 2009.

Tullen, P.: Méthodes d’analyse du fonctionnement hydrogéologique des versants instables, PhD thesis, EPFL, Lausanne. [online] Available from: http://infoscience.epfl.ch/record/33098, 2002.

Vallet, A., Bertrand, C. and Mudry, J.: Effective rainfall: a significant parameter to improve understanding of deep-seated rainfall triggering landslide - a simple computation temperature based method applied to Séchilienne unstable slope (French Alps), Hydrology and Earth System Sciences Discussions, 10(7), 8945–8991, doi:10.5194/hessd-10-8945-2013, 2013.

Vengeon, J.-M.: Déformation et rupture des versants en terrain métamorphique anisotrope: Apport de l’étude des Ruines de Séchilienne, PhD thesis, Université Joseph Fourrier I, Grenoble, 3 November., 1998.

Table 1: Analytical data (average values) of water samples: physico-chemical parameters and major ions. HF: Hydrochemical facies, SN: Samples number, Temp : temperature (°C), EC: electrical conductivity (µS/cm), ionic concentrations in meq/L., n.a. = Non-Analysed.

HF	Station ID	Water Type	SN	Temp. (field)	pH (field)	EC (field)	Ca meq/l	Mg meq/l	Na meq/l	K meq/l	Cl meq/l	HCO_3 meq/l	SO_4 meq/l	SiO_2 mmol/l
1	PLE	Ca-HCO_3	5	10.22	7.72	120.00	0.88	0.21	0.09	0.01	0.03	0.86	0.16	0.14
2	AIL	Mg-Ca- HCO_3	5	10.30	7.57	202.80	1.05	0.93	0.15	0.01	0.06	1.59	0.41	0.17
	MOU	Mg-Ca- HCO_3	5	13.66	7.86	367.00	1.95	1.87	0.18	0.02	0.08	3.04	0.75	0.16
	MTJ	Mg-Ca- HCO_3	2	9.90	7.75	440.50	2.50	2.32	0.14	0.02	0.04	3.75	1.06	0.15
	CMJ	Mg-Ca- HCO_3	4	11.47	7.94	455.80	2.59	2.32	0.16	0.02	0.04	3.84	1.12	0.16
	COR	Mg-Ca- HCO_3	4	12.10	7.52	538.80	2.69	3.16	0.19	0.02	0.06	4.28	1.62	0.16
3	G585-3	Mg-Ca- HCO_3-SO_4	1	10.10	7.05	314.00	1.55	2.09	n.a.	n.a.	0.33	2.64	1.03	n.a
	G585-2	Mg-Ca- HCO_3-SO_4	2	10.55	7.44	446.00	2.03	3.04	n.a.	n.a	0.07	2.92	2.29	n.a
	G585-1	Mg-Ca-SO_4- HCO_3	3	10.10	7.37	629.70	2.22	5.07	n.a.	n.a	0.06	3.47	3.92	0.14
	G710-2	Mg-Ca-SO_4- HCO_3	4	11.75	8.08	872.50	5.10	4.79	0.26	0.04	0.05	3.43	5.88	0.12
	G710-1	Mg-Ca-SO_4	4	12.10	7.67	384.30	1.98	1.80	0.21	0.05	0.05	0.61	3.18	0.23
4	VIZ1	Ca Mg-HCO_3-SO_4	5	11.22	7.56	354.80	2.88	0.68	0.21	0.02	0.18	2.05	1.36	0.12
	THE	Ca Mg-HCO_3-SO_4	5	11.50	7.77	332.20	2.31	1.07	0.15	0.01	0.09	2.51	0.80	0.13
	THL	Ca Mg-HCO_3-SO_4	5	11.24	7.54	465.20	3.53	1.42	0.13	0.02	0.09	3.25	1.58	0.12
	CBE	Ca Mg-HCO_3-SO_4	5	8.92	7.63	481.80	4.06	1.21	0.10	0.01	0.13	3.87	1.36	0.12
	BAT	Ca Mg-HCO_3-SO_4	3	12.00	7.70	499.70	3.99	1.33	0.12	0.01	0.06	3.40	1.93	0.12
	MAT	Ca Mg-HCO_3-SO_4	5	10.66	7.50	521.20	4.25	1.41	0.12	0.02	0.06	3.58	1.97	0.12
	FON	Ca Mg-HCO_3-SO_4	5	8.62	7.85	522.40	4.20	1.46	0.10	0.02	0.03	3.30	2.30	0.12

Table 2: Theoretical composition of different phases and initial solution (rain water composition from Atteia (1994)) employed in the inverse model. Composition of final solutions are given in table 1 (MTJ, CHJ, COR and G710-2).

Minerals	Stoechiometric formulae	Initial solution	
Albite	$NaAlSi_3O_8$	Temp (°C)	20
Muscovite	$KAl_3Si_3O_{10}(OH)_2$	pH	6
Clinochlore-14A	$Mg_5Al_2Si_3O_{10}(OH)_8$	Ca (meq/L)	3.85E-02
Phlogopite	$KAlMg_3Si_3O_{10}(OH)_2$	Mg (meq/L	4.42E-02
phengite	$K_{0.6}Mg_{0.25}Al_{1.8}Al_{0.5}Si_{3.5}O_{10}(OH)_2$	Na (meq/L	7.39E-03
Calcite	$CaCO_3$	K (meq/L	1.25E-03
dolomite	$CaMg(CO_3)_2$	Fe (meq/L	5.45E-05
Goethite	FeO(OH)	Al (meq/L	1.15E-04
O_2(g)	O_2	S(6) (meq/L	1.50E-02
CO_2(g)	CO_2	Cl (meq/L	equilibrate
		HCO_3 (meq/L	2.41E-02
		SiO_2 (mmol/L	5.30E-01

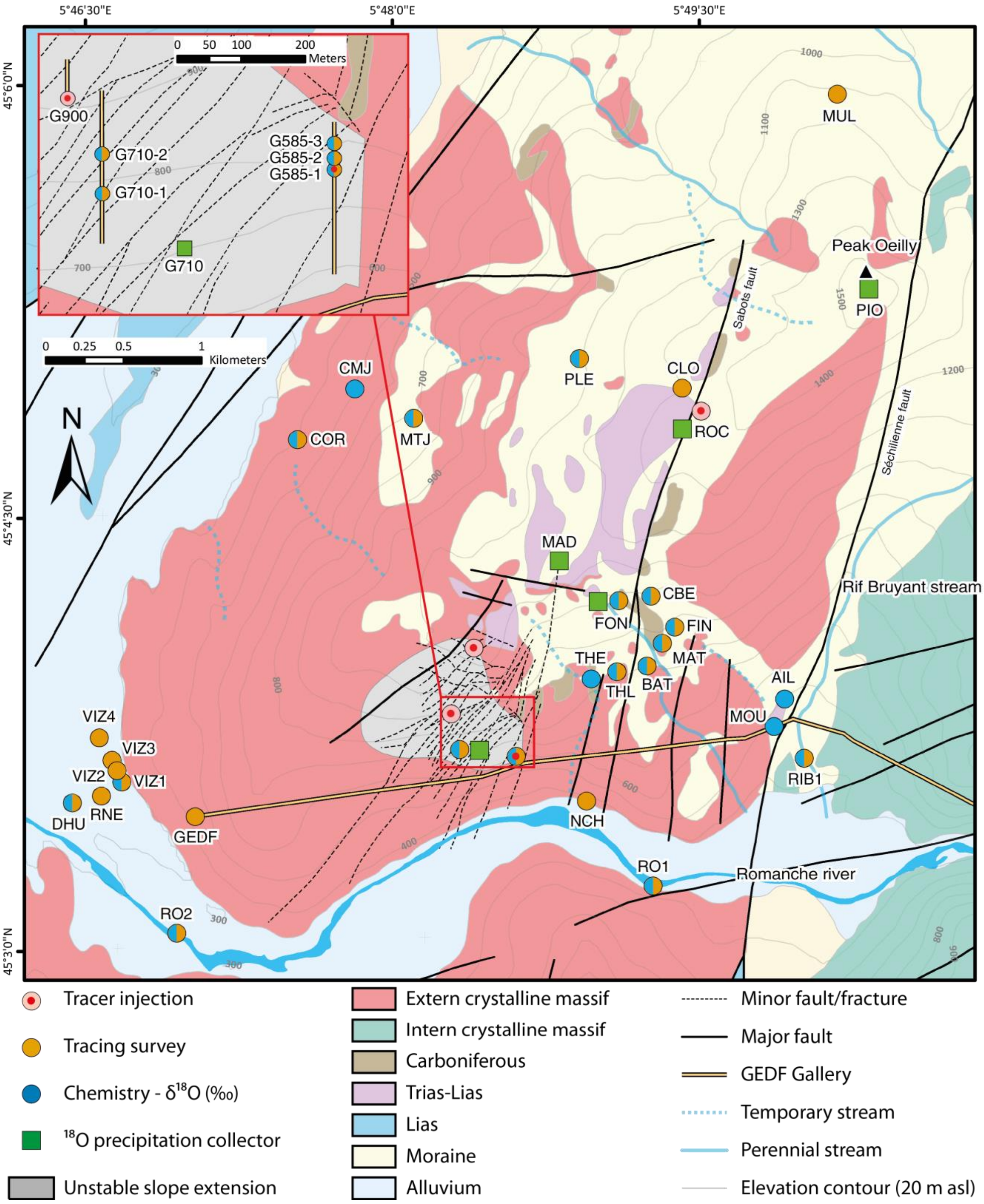

Figure 1: Site map and monitoring network

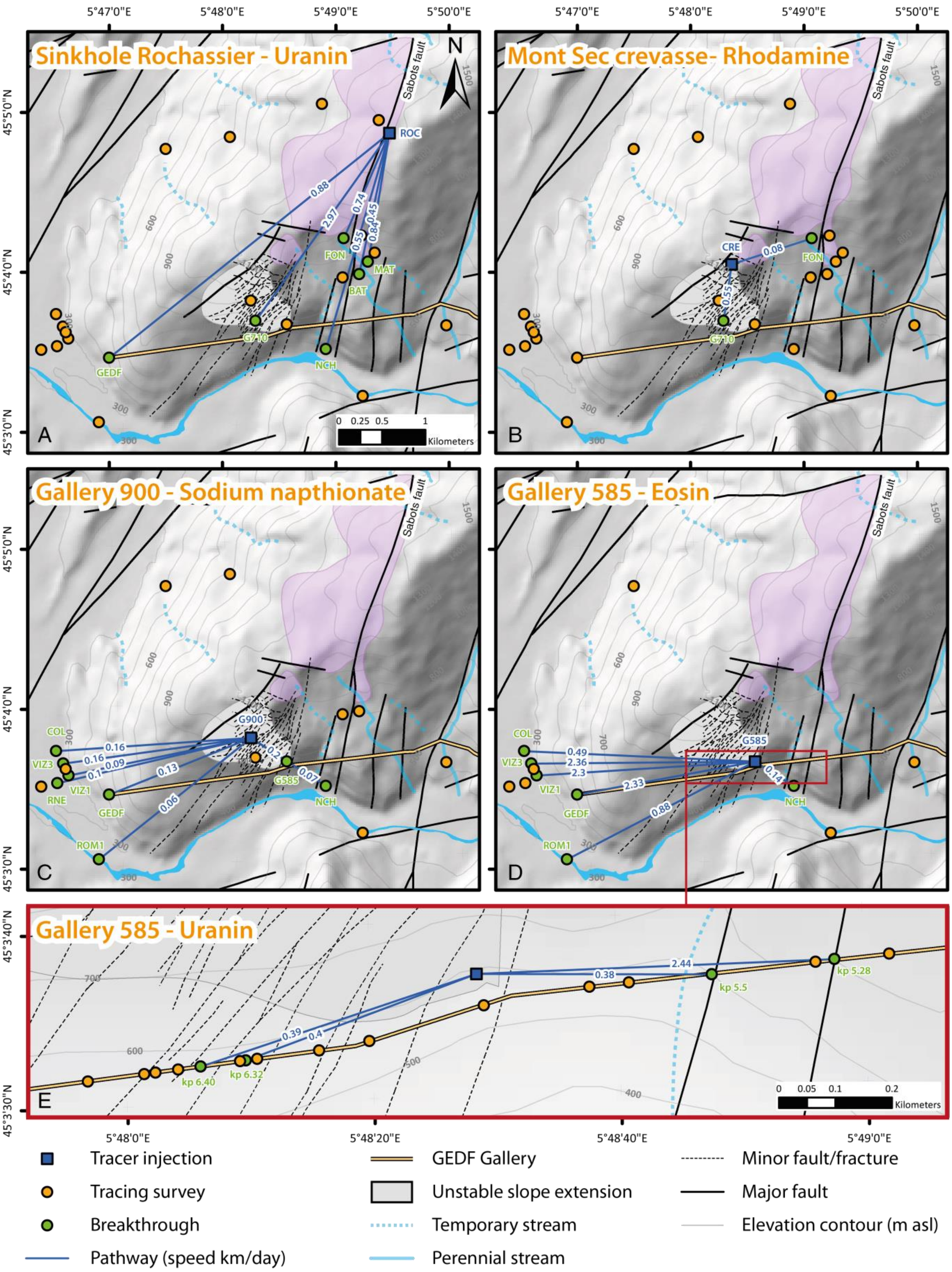

Figure 2: Tracer-tests analysis of April 2002 and March 2003 campaigns

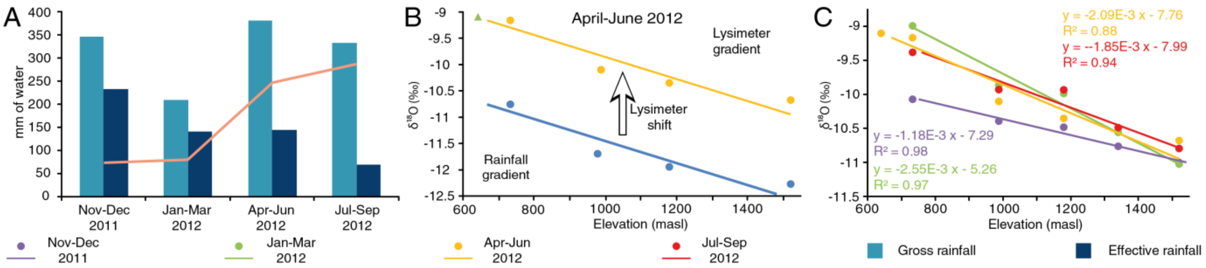

Figure 3: Isotope gradient and lysimeter shift

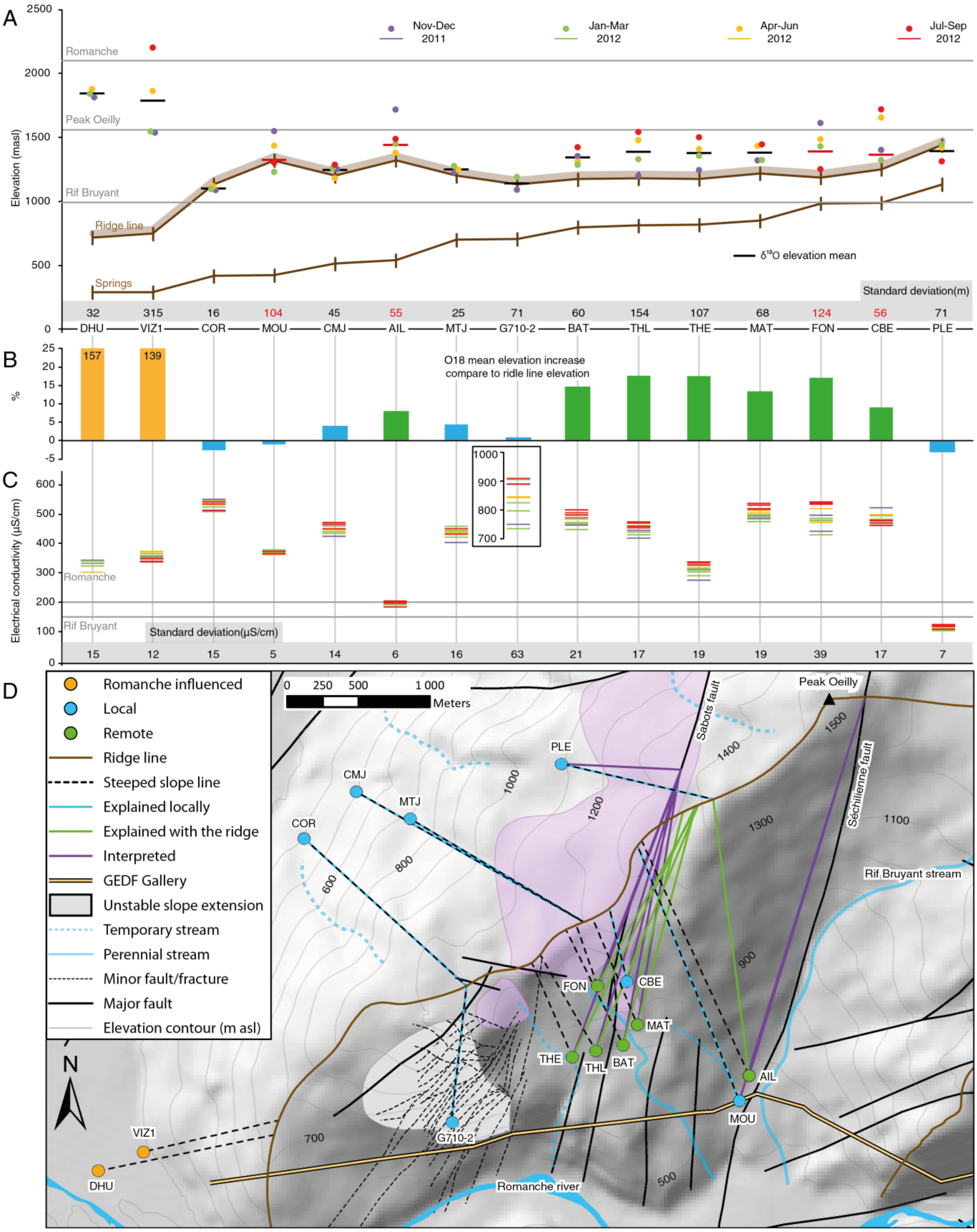

Figure 3: Seasonal analysis of water stable isotopes and conductivity

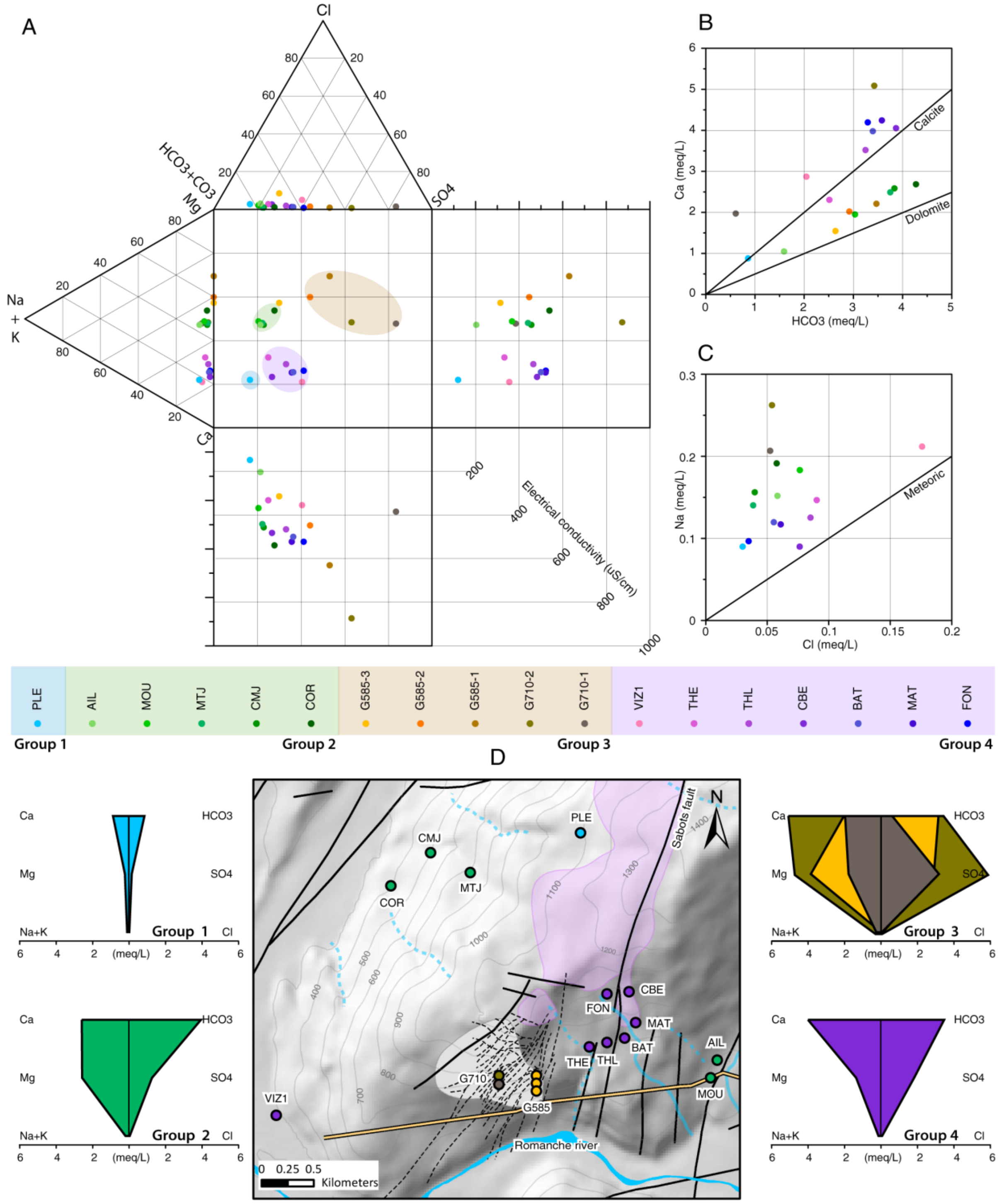

Figure 5: Hydrochemistry analysis

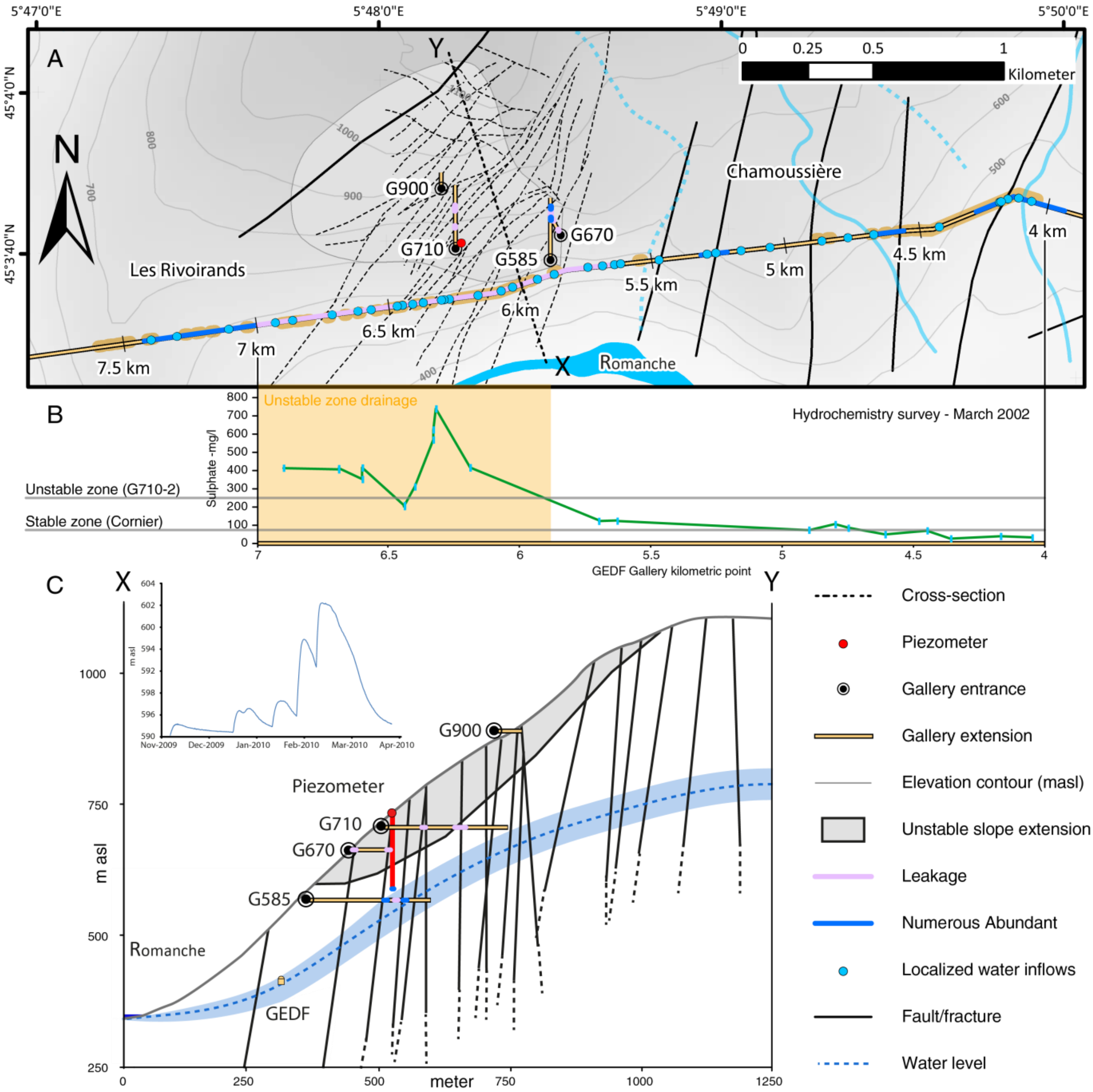

Figure 6: Galleries survey

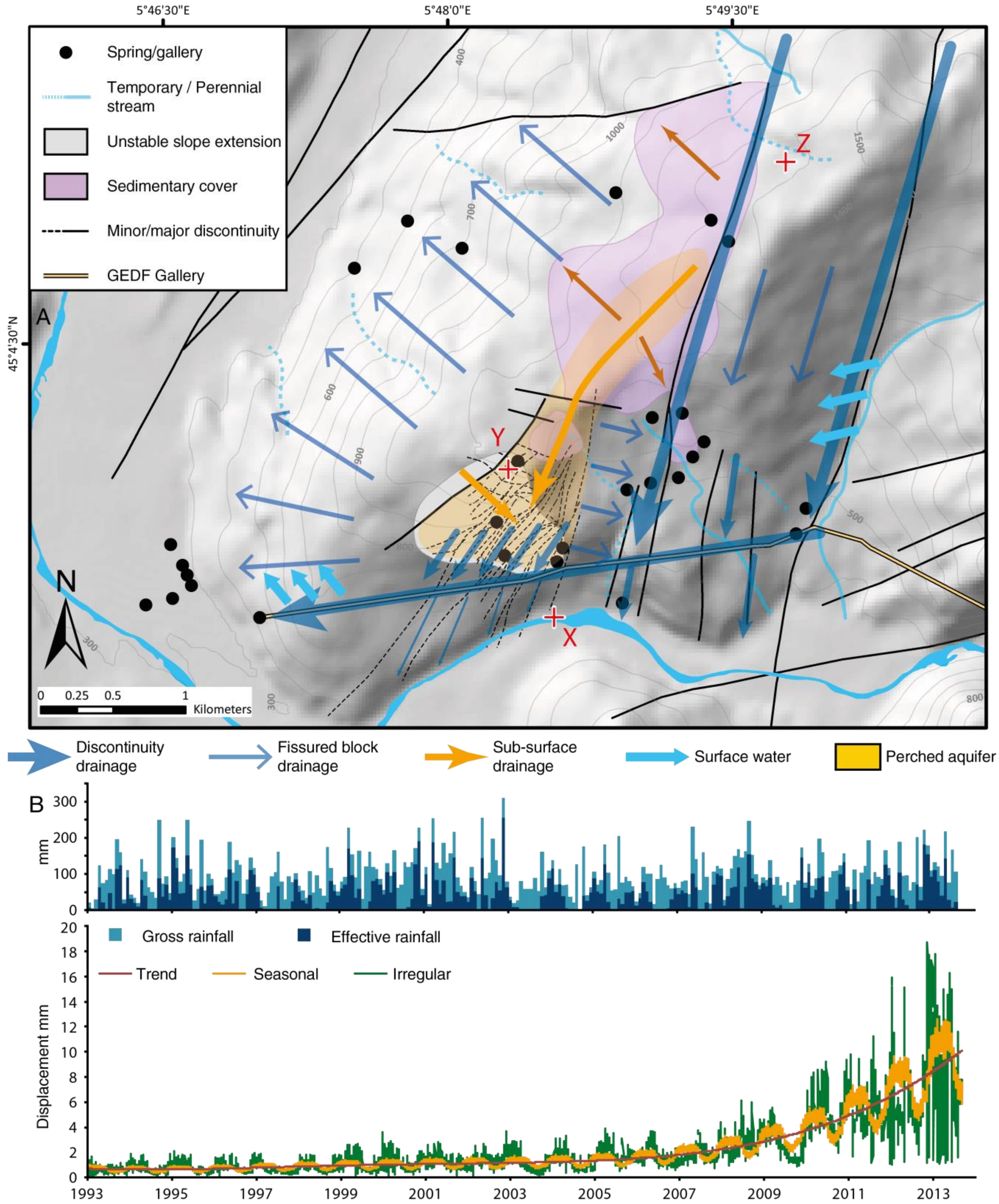

Figure 7: Groundwater flow scheme